Article

Molecular Cell

Codon Usage and 3′ UTR Length Determine Maternal mRNA Stability in Zebrafish

Graphical Abstract

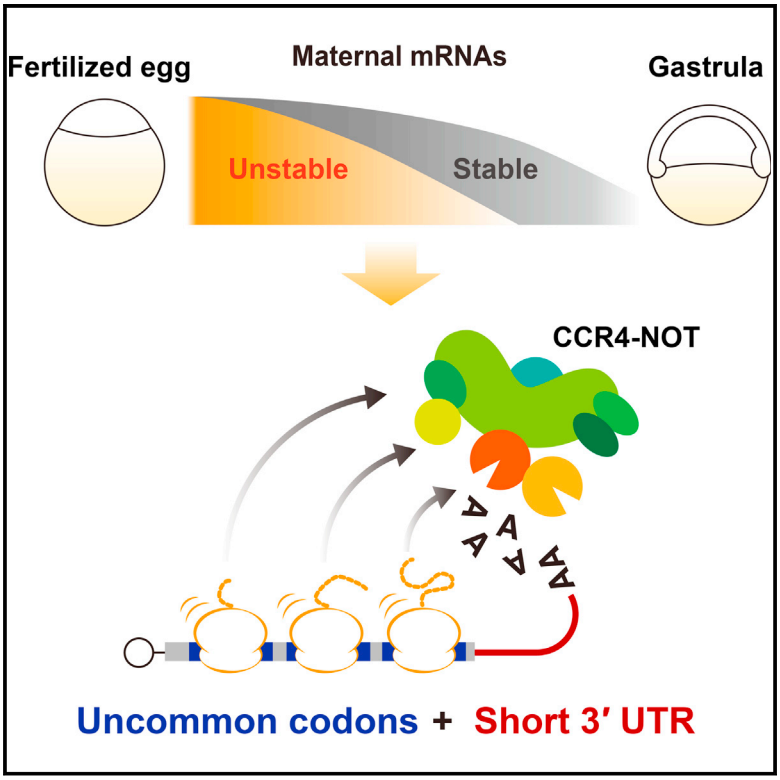

Authors

Yuichiro Mishima, Yukihide Tomari

Correspondence

mishima@iam.u-tokyo.ac.jp

In Brief

Mishima and Tomari show that codon usage determines the stability of maternal mRNAs during the maternal-to-zygotic transition in zebrafish. This codon-mediated mRNA decay is dependent on the CCR4-NOT deadenylase complex and is promoted by short 3′ UTRs.

Highlights

- Codon usage is a major determinant of maternal mRNA stability in zebrafish
- Codon-mediated mRNA decay is dependent on translation and the CCR4-NOT complex
- 3′ UTR length acts as a modulatory element for codon-mediated deadenylation

Accession Numbers

GSE71609

Mishima & Tomari, 2016, Molecular Cell *61*, 874–885
March 17, 2016
http://dx.doi.org/10.1016/j.molcel.2016.02.027

CellPress

CellPress

Molecular Cell
Article

Codon Usage and 3′ UTR Length Determine Maternal mRNA Stability in Zebrafish

Yuichiro Mishima[1,2,*] and Yukihide Tomari[1,2]
[1]Institute of Molecular and Cellular Biosciences
[2]Department of Computational Biology and Medical Sciences, Graduate School of Frontier Sciences
The University of Tokyo, 1-1-1, Yayoi, Bunkyo-ku, Tokyo 113-0032, Japan
*Correspondence: mishima@iam.u-tokyo.ac.jp
http://dx.doi.org/10.1016/j.molcel.2016.02.027

SUMMARY

The control of mRNA stability plays a central role in regulating gene expression. In metazoans, the earliest stages of development are driven by maternally supplied mRNAs. The degradation of these maternal mRNAs is critical for promoting the maternal-to-zygotic transition of developmental programs, although the underlying mechanisms are poorly understood in vertebrates. Here, we characterized maternal mRNA degradation pathways in zebrafish using a transcriptome analysis and systematic reporter assays. Our data demonstrate that ORFs enriched with uncommon codons promote deadenylation by the CCR4-NOT complex in a translation-dependent manner. This codon-mediated mRNA decay is conditional on the context of the 3′ UTR, with long 3′ UTRs conferring resistance to deadenylation. These results indicate that the combined effect of codon usage and 3′ UTR length determines the stability of maternal mRNAs in zebrafish embryos. Our study thus highlights the codon-mediated mRNA decay as a conserved regulatory mechanism in eukaryotes.

INTRODUCTION

Fertilization initiates an array of developmental programs that transform a single egg into an individual organism. The earliest stages of animal development are driven by maternally supplied mRNAs because transcription from the zygotic genome is quiescent immediately after fertilization. Subsequently, the zygotic genome is activated (zygotic genome activation, ZGA) and a subset of maternal mRNAs is degraded during a phase called the maternal-to-zygotic transition (MZT) (Tadros and Lipshitz, 2009). Precise clearance of maternal mRNAs during MZT is essential to prevent the inappropriate expression of maternal programs during zygotic stages. In addition, maternal mRNA clearance is unique in scale. In *Drosophila melanogaster*, for example, ~65% of protein-coding genes are expressed as maternal mRNAs, and ~35% of these mRNAs are degraded during MZT (De Renzis et al., 2007; Tadros et al., 2007). Therefore, maternal mRNA clearance is a dynamic renewal process of the gene expression profile.

Initial studies in *Drosophila* suggested that maternal mRNA clearance occurs through two major pathways: a pathway programed with maternal factors (maternal decay pathway) and a pathway activated by zygotic factors (zygotic decay pathway) (Bashirullah et al., 1999). Subsequent transcriptome analyses have confirmed these pathways in multiple organisms (Hamatani et al., 2004; Mathavan et al., 2005; Tadros et al., 2007; De Renzis et al., 2007). A limited number of molecular mechanisms that promote maternal mRNA clearance have been characterized. In the *Drosophila* maternal decay pathway, the RNA-binding protein Smaug promotes maternal mRNA clearance by binding to specific *cis*-acting elements (Tadros et al., 2007). Conversely, in the zebrafish zygotic decay pathway, the microRNA (miRNA) miR-430 is transcribed at ZGA and destabilizes ~400 maternal mRNAs via the target sequence GCACUU (Giraldez et al., 2006). miRNAs also play a role in the *Drosophila* zygotic decay pathway, although their sequences differ from that of miR-430 (Bushati et al., 2008). Additional factors and sequence elements have been identified in *C. elegans* (Stoeckius et al., 2014) and *X. laevis* (Paillard et al., 1998). Despite this progress, the mechanisms and factors responsible for the clearance of maternal mRNAs remain largely uncharacterized in vertebrates; even the best-studied example, miR-430, explains ~10% of maternal mRNA clearance in zebrafish (Giraldez et al., 2006) (see below).

mRNAs are degraded by either a general mRNA decay pathway or specific mRNA decay machineries. The shortening of the poly(A) tail, or deadenylation, is the first rate-limiting step in the general mRNA decay pathway. Deadenylation is mediated by two cytoplasmic deadenylase complexes, PAN2-PAN3 and CCR4-NOT (Chen and Shyu, 2011). The CCR4-NOT complex also interacts with Lsm1–Lsm7, PATL1, and decapping machineries to orchestrate mRNA deadenylation and decapping (Jonas and Izaurralde, 2013). The resulting deadenylated and decapped intermediates are subsequently degraded by the exonucleases Exosome and XRN1 (Decker and Parker, 2012).

Several mechanisms promote one or multiple steps of the general mRNA decay pathway for specific mRNAs. For example, miRNAs form a complex with the proteins Argonaute and GW182/TNRC6 and bind to complementary target mRNAs (Jonas and Izaurralde, 2015). GW182/TNRC6 further recruits the PAN2-PAN3 and CCR4-NOT deadenylase complexes, thereby promoting the deadenylation and degradation of target mRNAs (Chen et al., 2009; Braun et al., 2011; Chekulaeva

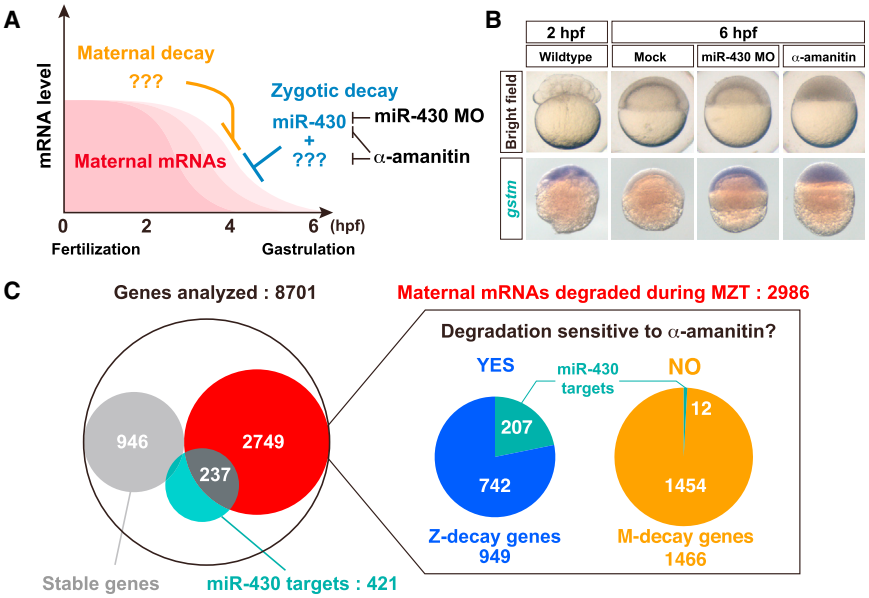

Figure 1. Classification of Maternal mRNA Decay Pathways in Zebrafish

(A) A schematic representation of maternal mRNA decay pathways in zebrafish.

(B) Bright field pictures (upper panels) and in situ hybridization to detect *gstm* mRNA (lower panels, purple) in wild-type, miR-430 MO-injected, and α-amanitin-injected embryos.

(C) Left: a Venn diagram of the result of the RNA sequencing analysis. Right: pie charts representing subclasses of maternal genes whose mRNAs are degraded during MZT. The numbers show genes in each subclass.

(D) qRT-PCR analysis of wild-type and α-amanitin-injected embryos. mRNA levels at 0 hpf were set to one. The graph represents an average of three independent injection experiments. The error bars show SD.

(E) In situ hybridization to detect mRNAs of M-decay genes *suv39h1a* (upper panels) and *pus1* (lower panels) in wild-type and α-amanitin-injected embryos. See also Figure S1.

et al., 2011; Fabian et al., 2011). Analogously, sequence-specific RNA-binding proteins, such as TTP, Smaug, and Nanos, recruit the CCR4-NOT complex to promote the degradation of their target mRNAs (Semotok et al., 2005; Suzuki et al., 2010; Sandler et al., 2011). More generally, the combination of *cis* elements in mRNAs and specific RNA-binding factors that recruit mRNA decay machineries is a widespread mode for the control of mRNA stability in eukaryotes (Chen and Shyu, 2011).

In contrast to the *cis*-element-based scenario, the ribosome recognizes some features of the ORF and triggers mRNA degradation. mRNA quality control systems, such as nonsense-mediated decay (NMD), no-go decay (NGD), and nonstop decay (NSD), monitor premature termination or stall of the ribosome and promote mRNA decay (Lykke-Andersen and Bennett, 2014). The fitness of codons for translation, or codon optimality, has recently been identified as a determinant of mRNA stability in yeast (Presnyak et al., 2015). Because codon optimality correlates with tRNA availability (Chaney and Clark, 2015), it was hypothesized that the rate of codon decoding by the ribosome affects mRNA stability. Codon-mediated decay is dependent on the CCR4-NOT deadenylase complex and the decapping enzyme Dcp2 but does not require the components of NMD and NGD (Presnyak et al., 2015). These observations indicate that codon-mediated decay is a unique cotranslational mRNA degradation pathway mediated by deadenylation and decapping. However, the generality of codon-mediated mRNA decay in eukaryotes and the impact of this decay on gene expression patterns under complex biological processes remain unknown.

Here, we deciphered the maternal mRNA clearance pathway in vertebrates using zebrafish as a model system. Using transcriptome analyses, we discriminated maternal and zygotic decay pathways in zebrafish, both of which are largely dependent on deadenylation by the CCR4-NOT complex. We demonstrated that the ORF of mRNAs degraded via the maternal decay pathway is enriched with uncommon synonymous codons and triggers deadenylation in a translation-dependent manner. Furthermore, the effect of uncommon codons depends on the length of the 3′ UTR. These results indicate that codon-mediated mRNA decay is conserved in eukaryotes and is utilized for the selective clearance of a subset of maternal mRNAs in zebrafish.

RESULTS

Classification of the Maternal mRNA Clearance Pathways in Zebrafish

To better characterize maternal mRNA clearance during zebrafish MZT, we performed RNA sequencing of pre-MZT (Figure 1A; 2 hr postfertilization, hpf) and post-MZT embryos (Figure 1A; 6 hpf; note that ZGA occurs at 2.75 hpf in zebrafish; Kane and Kimmel, 1993). To distinguish maternal and zygotic decay pathways, we included two additional conditions at 6 hpf. The zygotic decay factors miR-430a–c (Giraldez et al., 2006) were inhibited by specific morpholino antisense oligos (MOs) (Figures 1A and S1A, available online), or the entire zygotic transcription program was inhibited by the RNA polymerase II inhibitor α-amanitin (Figures 1A and S1B). miR-430 MOs and α-amanitin induced

mild and severe gastrulation defects, respectively, and the accumulation of the miR-430 target mRNA *gstm* (Figure 1B) (Giraldez et al., 2006). RNA sequencing was performed in triplicate under each condition using the rRNA-depletion method to analyze changes in mRNA amount apart from changes in the poly(A) tail length (Presnyak et al., 2015). Genes with reliable sequence annotation and >1 RPKM in post-MZT embryos were further analyzed (see Supplemental Experimental Procedures).

Among the 8,701 genes analyzed, those with significant decreases in mRNA levels of more than 2-fold between pre-MZT and post-MZT embryos were considered maternal mRNAs degraded during MZT (Figure 1C; 2,986 genes). miR-430 target genes were independently identified by comparison with post-MZT wild-type embryos and miR-430 MO-injected embryos. Based on a previous analysis of MZ*dicer* mutant embryos, genes that exhibited more than 1.5-fold upregulation of mRNA levels in the absence of miR-430 and had at least one 6-mer seed-matched site were considered direct miR-430 target genes (Giraldez et al., 2006) (Figure 1C; 421 genes). Of those miR-430 targets, 237 genes encoded unstable maternal mRNAs, consistent with the previous study (Giraldez et al., 2006). We next classified unstable maternal mRNAs into two decay pathways based on the response to α-amanitin. Genes whose mRNA levels increased more than 2-fold in α-amanitin-injected 6 hpf embryos compared with post-MZT embryos (i.e., mRNAs that were stabilized in the absence of zygotic transcription) were identified as zygotic decay genes (Figure 1C, Z-decay genes, 949). By contrast, genes whose mRNA levels decreased more than 2-fold in α-amanitin-injected 6 hpf embryos compared with pre-MZT embryos (i.e., mRNAs that were degraded independently of zygotic transcription) were considered maternal decay genes (Figure 1C, M-decay genes, 1,466). To maintain mutual exclusivity, overlapping genes between the two classes were excluded (111 genes). In addition to the two decay pathways, genes encoding mRNAs whose expression levels changed within a range of −0.3 to 0.3-fold (log2 scale) during MZT regardless of the α-amanitin treatment were identified as stable genes (Figure 1C, stable genes, 946).

We concluded that this classification accurately distinguished zygotic and maternal decay pathways based on the following observations. First, the miR-430 target sites were enriched in genes whose mRNA levels are upregulated by miR-430 MO and in Z-decay genes (Figures S1C and S1D), but not in stable and M-decay genes (Figures S1E and S1F). Second, the experimentally identified miR-430 target genes were mostly classified into Z-decay genes (Figure 1C; 207 genes in Z-decay genes). Third, qRT-PCR and in situ hybridization validated transcription-dependent and transcription-independent mRNA degradation (Figures 1D and 1E). Overall, these analyses provided a genome-wide view of the two maternal mRNA decay pathways in zebrafish. In the subsequent analysis, we focused on the M-decay genes because the mRNA degradation mechanisms of many of these genes have not been well characterized in vertebrates.

Maternal mRNAs Are Actively Deadenylated by the CCR4-NOT Complex

The poly(A) tails of maternal mRNAs are regulated dynamically in many animals (Weill et al., 2012). To analyze the poly(A) tail status of maternal mRNAs, we utilized poly(G/I) tailing-based PAT assay (Kusov et al., 2001), which can accurately recapitulate the changes of poly(A) tail lengths (Figures S2A–S2C) (Bazzini et al., 2012). This assay revealed that the stable mRNA *vasa* was polyadenylated >100 nt after fertilization, followed by gradual deadenylation as described previously (Figure 2A, *vasa*) (Mishima et al., 2006). The miR-430 target mRNA *eif4ebp2* was also polyadenylated after fertilization but rapidly lost its poly(A) tail after 3 hpf via miR-430-mediated deadenylation (Figure 2A, *eif4ebp2*) (Giraldez et al., 2006). By contrast, M-decay mRNAs *trmt11* and *suv39h1a* retained relatively short poly(A) tails from fertilization to 6 hpf (Figure 2A, *trmt11* and *suv39h1a*). Supporting the PAT assay, analysis of the previous poly(A) tail profiling data confirmed that the short poly(A) tail pattern is a common characteristic of M-decay genes (Figures S2D–S2F) (Subtelny et al., 2014). These observations reveal a unique poly(A) tail regulation of M-decay mRNAs that is distinct from those of stable mRNAs or miR-430 target mRNAs.

Either poor polyadenylation or enhanced deadenylation could explain the short poly(A) tails and subsequent degradation of M-decay mRNAs. To distinguish these possibilities, we inhibited the major cytoplasmic deadenylase CCR4-NOT by overexpressing a dominant-negative form of CNOT7 (CNOT7-DN), a catalytic subunit of the complex (Collart and Panasenko, 2012) (Figure S2G). CNOT7-DN lacks catalytic activity (D40A and E42A mutations; Bianchin et al., 2005) and cannot bind to the other catalytic subunit CNOT6/CCR4 (C67E and L71E mutations; Basquin et al., 2012) (Figures S2H and S2I), resulting in sequestration of the complex in an inactive state (Zheng et al., 2008; Makino et al., 2015). PAT assay revealed poly(A) tail lengthening of the two M-decay mRNAs in the presence of CNOT7-DN, indicating that the short poly(A) tail status of these M-decay mRNAs was the consequence of enhanced deadenylation by the CCR4-NOT complex (Figure 2B). Consistently, RNA sequencing of 6 hpf embryos revealed that CNOT7-DN induced the global accumulation of M-decay mRNAs as well as Z-decay mRNAs (Figure 2C). qRT-PCR validated that CNOT7-DN caused mRNA accumulation via the interaction with CNOT1, a scaffold protein of the CCR4-NOT complex (Figures 2D and S2H–S2J; the M141R mutation inhibits the interaction between CNOT7 and CNOT1; Petit et al., 2012). These results suggest a widespread impact of CCR4-NOT-mediated deadenylation on maternal mRNA clearance.

M-Decay mRNAs Are Degraded via Cotranslational Deadenylation

We next identified the determinant within M-decay mRNAs that induces deadenylation and degradation via the CCR4-NOT complex. However, whereas the miR-430 target sequence GCACUU was identified as the most enriched motif in Z-decay genes, we did not identify any common motifs in M-decay genes (Figure S3A; data not shown). Moreover, M-decay genes possessed shorter 3′ UTRs, whereas Z-decay and stable genes possessed longer 3′ UTRs than the "all genes" background (Figures 3A–3C). This bias was not attributable to the incomplete annotation of 3′ UTRs because the last 100 nucleotides (nt) sequences of this region, which should include polyadenylation signals (PASs) (Shi and Manley, 2015), were comparable between the three classes (Figure S3B). Furthermore, the number and types

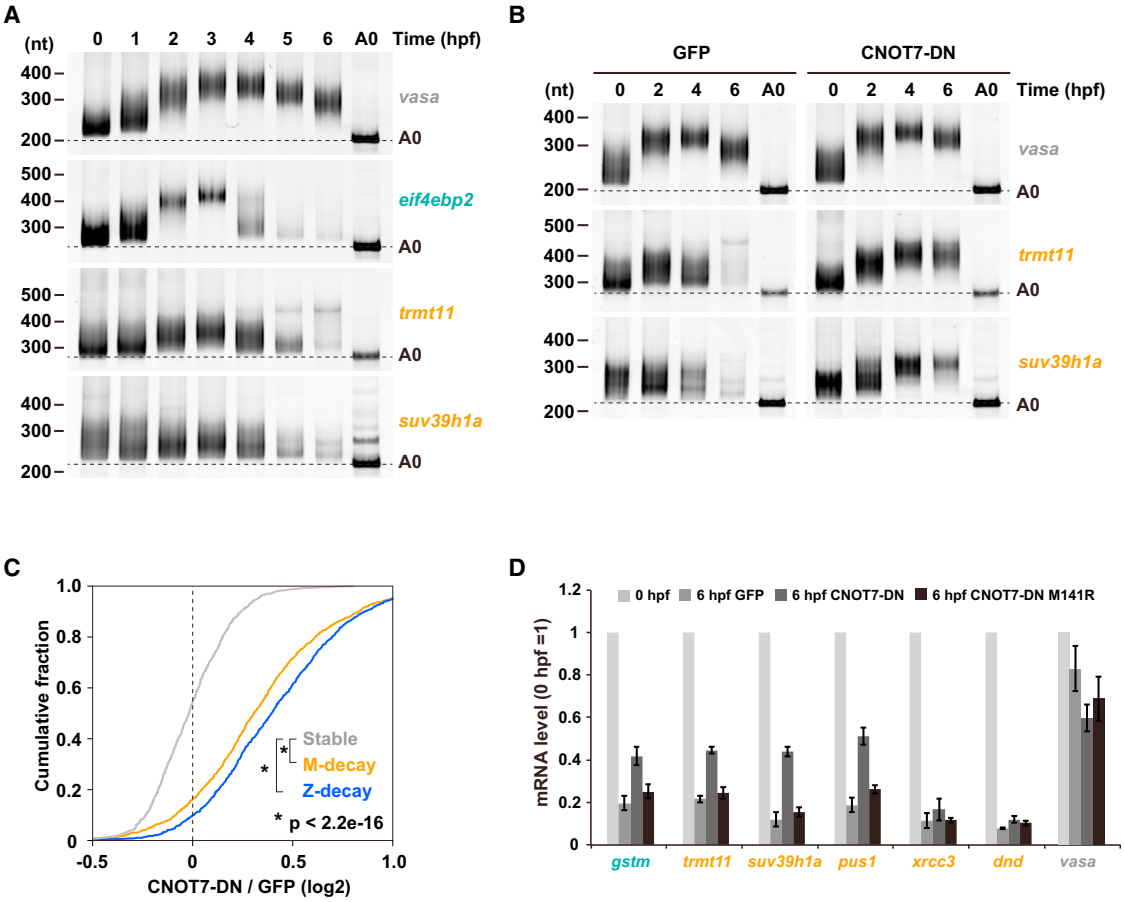

Figure 2. The Impact of the CCR4-NOT Complex on Maternal mRNA Deadenylation and Degradation

(A) Results of the time course PAT assay for *vasa*, *eif4ebp2*, *trmt11*, and *suv39h1a* mRNAs. The developmental stages are shown above as hpf. Lanes labeled as A0 show 3′ UTR fragments without a poly(A) tail.

(B) Results of the time course PAT assay for *vasa*, *trmt11*, and *suv39h1a* mRNAs in GFP- or CNOT7-DN-expressing embryos.

(C) A cumulative plot showing fraction of genes (y axis) and log2-fold changes of mRNA levels between EGFP- and CNOT7-DN-expressing 6 hpf embryos (x axis). Stable genes (gray), M-decay genes (orange), and Z-decay genes (blue) are shown. The p values compared with stable genes are shown (two-sided Kolmogorov-Smirnov test).

(D) qRT-PCR analysis of GFP-, CNOT7-DN-, or CNOT7-DN M141R-expressing embryos. mRNA levels at 0 hpf were set to one. The graph represents an average of three independent injection experiments. The error bars show SD. See also Figure S2.

of the putative PASs in the last 50 nt (Figures S3C and S3D) and the number of putative cytoplasmic polyadenylation elements (CPEs) in the last 100 nt (Ivshina et al., 2014) (Figure S3E) were nearly identical among the three classes. These observations suggest that the stability determinant of M-decay mRNAs is distinct from canonical *cis*-regulatory elements frequently embedded in the 3′ UTR (Chen and Shyu, 2011; Bartel, 2009).

To experimentally identify the determinant, we performed a reporter assay by injecting in vitro synthesized, capped, and nonadenylated mRNAs into one-cell stage embryos, followed by a time course PAT assay. We first examined EGFP mRNA containing a short 3′ UTR of the M-decay gene *suv39h1a* (174 nt). The reporter mRNA was polyadenylated after injection, but strong deadenylation was not observed (Figure 3D, left panel). Next, we included an ORF of *suv39h1a* as a fusion to the EGFP ORF. This reporter mRNA was polyadenylated after injection but lost the poly(A) tail at 6 hpf, suggesting that the *suv39h1a* ORF promoted deadenylation (Figure 3D, middle panel). To determine whether deadenylation is triggered by the ORF sequence per se or a cotranslational event on the ORF, we inhibited translation of the ORF using an MO that hybridizes to the EGFP translation start site (EGFP MO; Figure 3E). Strikingly, EGFP MO efficiently blocked deadenylation induced by the *suv39h1a* ORF (Figure 3D, right panel). Deadenylation was dependent on the translation of the *suv39h1a* ORF because substituting EGFP with Myc-tags did not affect cotranslational deadenylation (Figures S4A and S4B). Furthermore, a combination of the ORF and the 3′ UTR of another M-decay gene, *pus1*, also induced cotranslational deadenylation (Figures S4C and S4D). These results suggest that translation of the ORF of M-decay genes promotes deadenylation.

Next we examined the cotranslational deadenylation of endogenous mRNAs. The injection of a translation-blocking MO against endogenous *suv39h1a* mRNA strongly inhibited the deadenylation and degradation of the *suv39h1a* mRNA (Figures 3F–3H).

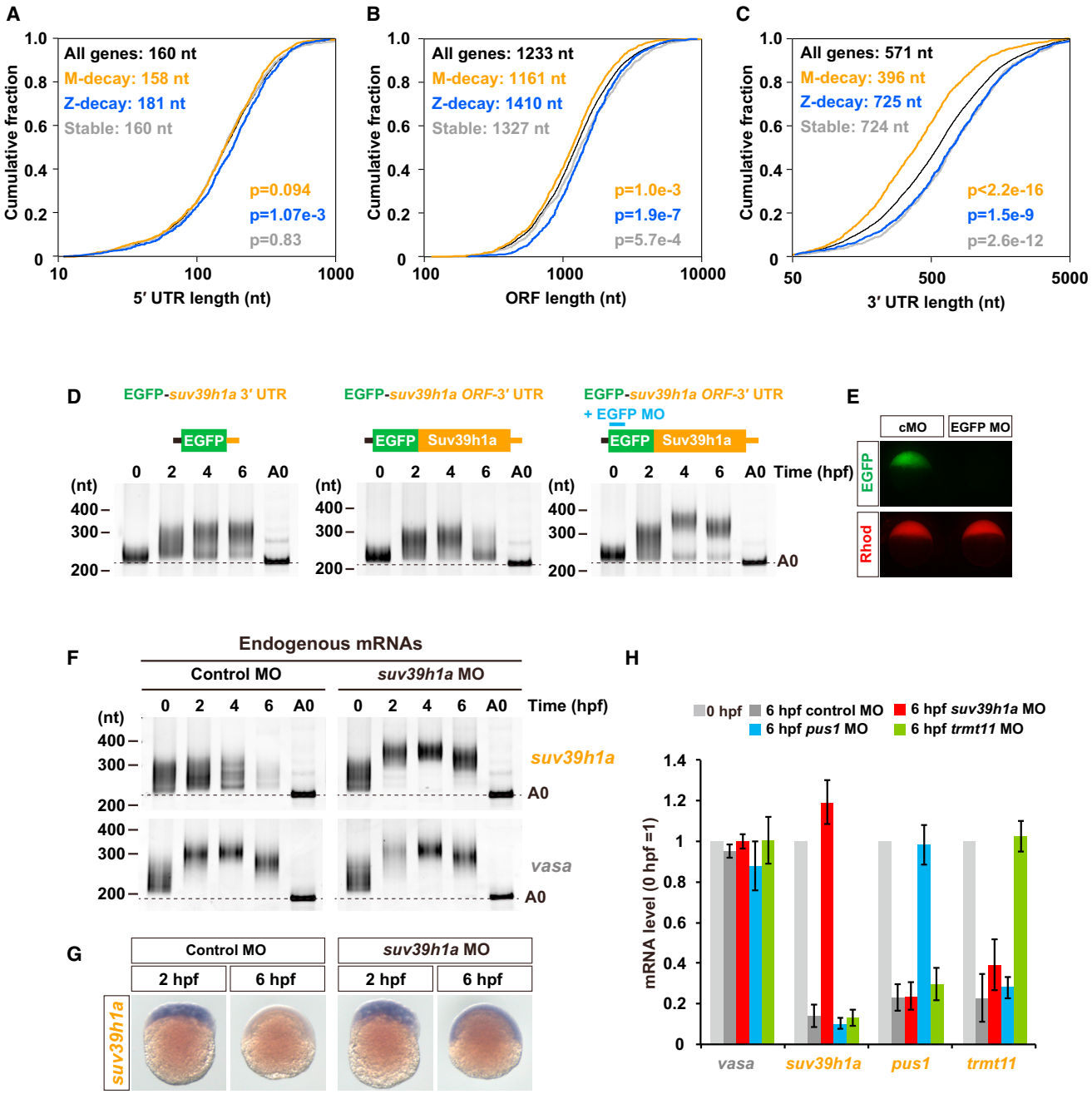

Figure 3. Cotranslational Deadenylation and Degradation of M-Decay mRNAs

(A–C) Cumulative plots showing the distributions of 5′ UTR (A), ORF (B), and 3′ UTR (C) length in all genes (black), Z-decay genes (blue), M-decay genes (orange), and stable genes (gray). The x axis shows the length of each region on a log10 scale. The y axis shows the cumulative fraction. The median length (upper left) and the p values compared with all genes (lower right, two-sided Kolmogorov-Smirnov test) are shown.

(D) Results of the time course PAT assay of EGFP reporter mRNAs injected at the one-cell stage. The developmental stages are shown above as hpf. Lanes labeled as A0 show 3′ UTR fragments without a poly(A) tail.

(E) GFP fluorescence of embryos injected with GFP reporter mRNA and control MO or EGFP MO (upper panel, green). The fluorescence of coinjected rhodamine-dextran is shown as an injection control (lower panel, red).

(F) Results of the time course PAT assay of *suv39h1a* and *vasa* mRNAs in embryos injected with control MO or *suv39h1a* MO.

(G) In situ hybridization detecting *suv39h1a* mRNA in control MO- or *suv39h1a* MO-injected embryos.

(H) qRT-PCR analysis of MO-injected embryos. The mRNA levels at 0 hpf were set to one. The graphs represent the averages of three independent injection experiments. The error bars show SD. See also Figures S3 and S4.

MOs against two other M-decay genes (*pus1* and *trmt11*) also inhibited mRNA degradation (Figure 3H), confirming the generality of the cotranslational degradation of M-decay mRNAs. By contrast, miR-430-dependent deadenylation and degradation of Z-decay mRNAs were not affected by MOs (Figures S4E and S4F), consistent with previous reports (Giraldez et al., 2006; Mishima et al., 2006). These results indicate that the stability and the deadenylation rate of M-decay mRNAs are defined by their ORFs in a translation-dependent manner.

Codon Usage Determines the Deadenylation Rate in Zebrafish Embryos

We attempted to identify the minimal region of the *suv39h1a* ORF responsible for cotranslational deadenylation, but partial fragments of the *suv39h1a* ORF were not sufficient to induce robust deadenylation when fused to the EGFP ORF (data not shown). We therefore hypothesized that features associated with a large portion of the ORF induce cotranslational deadenylation. One such example is synonymous codon usage, which affects various cotranslational events (Pechmann and Frydman, 2013; Presnyak et al., 2015; Yu et al., 2015; Chaney and Clark, 2015; Kim et al., 2015). To analyze synonymous codon usage in zebrafish, we utilized the codon adaptation index (CAI), a metric of the relative fitness of the synonymous codon usage compared with reference genes (Sharp and Li, 1987) (see Supplemental Experimental Procedures). Intriguingly, M-decay genes exhibited a lower CAI than all genes analyzed in the present study, indicating that the ORFs of M-decay genes are enriched with uncommon codons (Figure 4A). By contrast, stable genes exhibited a higher CAI and therefore were biased toward ORFs enriched with commonly used codons.

To experimentally evaluate the effect of synonymous codon usage on cotranslational deadenylation, we performed mRNA injection experiments. First, we artificially adapted the codon usage of the *suv39h1a* ORF to the most common codons without changing the encoded amino acid sequence (CAI 0.816 to 0.998). Indeed, the codon-adapted *suv39h1a* ORF exhibited tolerance to deadenylation (Figures 4B and 4C). Second, we systematically modified the synonymous codon usage of the human-optimized EGFP ORF (CAI 0.916). Although the human-optimized EGFP ORF fused to the *suv39h1a* 3′ UTR did not cause significant deadenylation (Figures 3D and 4D), the modified ORF promoted deadenylation when the CAI was decreased, with the CAI of 0.738 exhibiting the strongest effect (Figure 4D). Deadenylation was indeed promoted cotranslationally because the inhibition of translation by EGFP MO diminished deadenylation (Figure 4D, + EGFP MO). Differential deadenylation patterns of the EGFP variant mRNAs were further confirmed by coinjecting a mixture of the four EGFP variant mRNAs and performing variant-specific PAT assays (Figures 4E, 4F, and S5A). Consistent with these deadenylation patterns, we observed a difference of EGFP fluorescence intensity between the most codon-adopted and the least codon-adapted EGFP reporters at later stages (Figure S5B). Third, we focused on the leucine codons to analyze the effect of synonymous codon usage on deadenylation with minimal changes in the ORF sequence. Leucine is specified by six codons, of which CUG is the most common and CUA is the least common in zebrafish (Figure 4G). The EGFP (CAI = 0.835) ORF, which did not induce strong deadenylation (Figure 4D), contains 21 leucine codons, all of which are specified by CUG. The substitution of these 21 CUG codons with CUA codons was sufficient to induce deadenylation (Figures 4H and 4I). Taken together, these results demonstrate that synonymous codon usage of the ORF determines the deadenylation rate in zebrafish embryos.

A Long 3′ UTR Confers Resistance to Codon-Mediated Deadenylation

Although codon-mediated mRNA deadenylation is evident in our reporter assay, 43% of stable genes displayed a CAI below the median of all genes (Figure 4A). We therefore reasoned that there might be an additional factor that affects the efficiency of codon-mediated deadenylation. The length of the 3′ UTR is a candidate for such a factor because we detected inverse 3′ UTR length bias between M-decay and stable genes (Figure 3C). To examine the effect of 3′ UTR contexts on codon-mediated deadenylation, we performed 3′ UTR-swapping experiments. Instead of the 174-nt 3′ UTR of the M-decay gene *suv39h1a*, the 640-nt 3′ UTR of the stable gene *vasa* was fused to the codon-modified EGFP ORFs. PAT assays revealed that the 3′ UTR of *vasa* resisted codon-mediated deadenylation, even with the EGFP ORF with a CAI of 0.775 (Figure 5A; note that the corresponding reporter mRNA with the *suv39h1a* 3′ UTR was deadenylated). By contrast, a reporter mRNA with the least optimal EGFP ORF (CAI 0.738), followed by the *vasa* 3′ UTR, was deadenylated by 6 hpf, likely reflecting the strong deadenylation activity of the ORF (CAI 0.738 corresponds to the 100th percentile in all genes analyzed) rather than the difference in the translation activity (Figure S5C). These observations indicate that codon-mediated deadenylation is dependent on the context of the 3′ UTR.

To determine whether the length of the 3′ UTR rather than the sequence confers resistance to codon-mediated deadenylation, we systematically extended the length of the 3′ UTR in the EGFP (CAI 0.775)-*suv39h1a* 3′ UTR reporter mRNA by inserting shuffled 3′ UTR sequences (Figure 5B). Lengthening the 3′ UTR from 174 nt to 600 or 900 nt suppressed codon-mediated deadenylation, whereas extending the 3′ UTR to 300 nt did not (Figures 5C–5E). This effect was independent of the primary sequence because the extension of the 3′ UTR to 600 nt using an antisense sequence also suppressed deadenylation (Figure S5D). These experiments indicate that a long 3′ UTR confers resistance to codon-mediated deadenylation in zebrafish embryos.

We hypothesized that a long 3′ UTR increases the distance from uncommon codons to the 3′ end, thereby decreasing the accessibility of the machinery for codon-mediated decay to the poly(A) tail (distance model). If this is the case, increasing the distance between uncommon codons and the poly(A) tail by changing the position of uncommon codons within the ORF should mimic the inhibitory effect of a long 3′ UTR. To investigate this possibility, we placed uncommon codons locally at either the 5′ or the 3′ of ORF by combining high CAI (CAI = 0.835) and low CAI (CAI = 0.738) EGFP ORFs (Figures 5F–5H, 3′ low and 5′ low). Consistent with the distance model, PAT assay revealed that codon-mediated deadenylation occurred more efficiently when uncommon codons were placed at the 3′ end of the ORF. This effect correlated with the proximity of uncommon

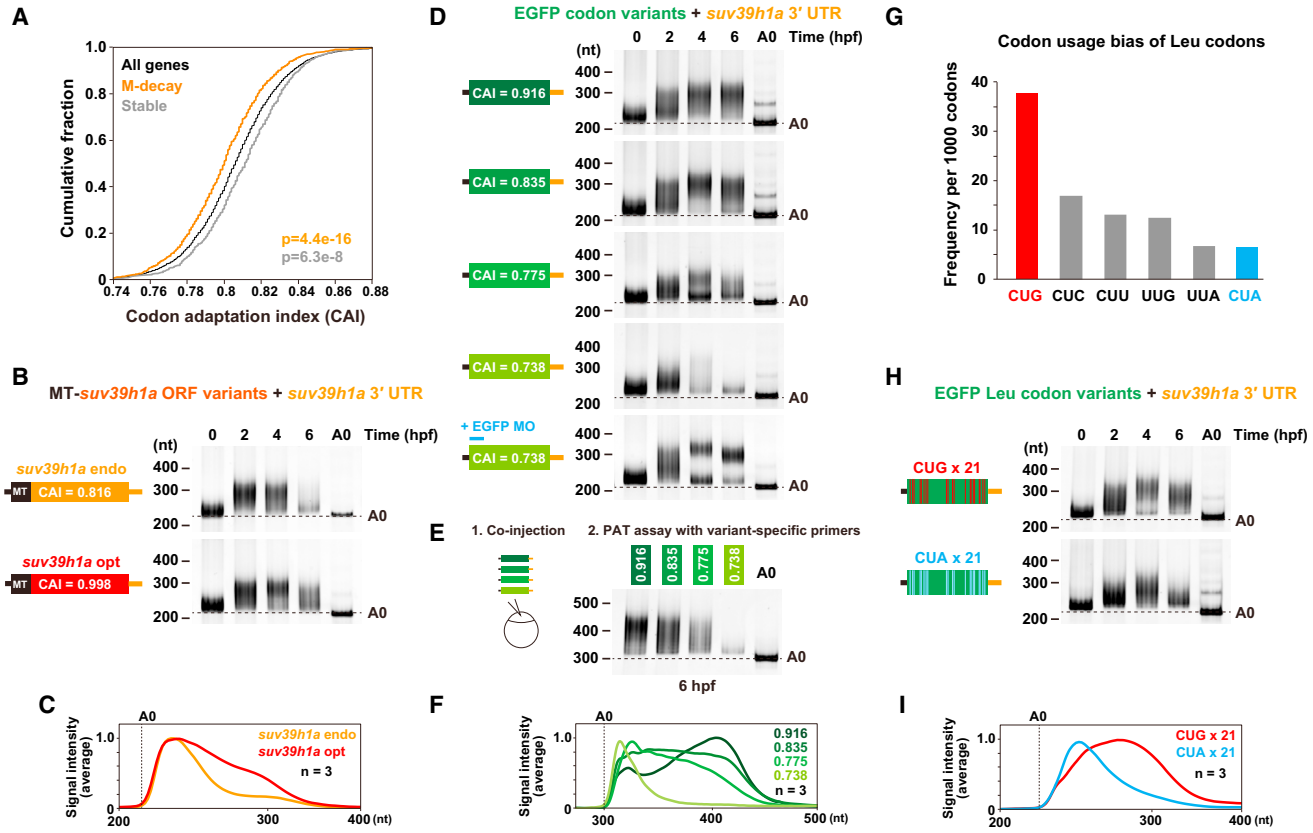

Figure 4. The Impact of Codon Usage Bias on mRNA Deadenylation in Zebrafish Embryos

(A) Cumulative plots of CAI in all genes (black), M-decay genes (orange), and stable genes (gray). The x axis shows the CAI, and the y axis shows the cumulative fraction. The p values compared with all genes are shown (lower right, two-sided Kolmogorov-Smirnov test).

(B) Results of the time course PAT assay for Myc-tagged (MT) *suv39h1a* reporter mRNAs containing an endogenous ORF (orange) or a codon-adapted ORF (red) followed by the *suv39h1a* 3′ UTR. CAI is shown in white letters. Developmental stages are shown above as hpf. Lanes labeled as A0 show 3′ UTR fragments without a poly(A) tail.

(C) Quantification of the PAT assay in (B) at 6 hpf. The plots show the averaged relative signal intensity of three biological replicates (y axis) and the mobility (x axis).

(D) Results of the time course PAT assay for reporter mRNAs containing EGFP ORF with differential synonymous codon usage (shown as a green gradient; CAI is shown in white letters) followed by the *suv39h1a* 3′ UTR.

(E) Results of the PAT assay at 6 hpf for the four EGFP variant mRNAs used in (D) but coinjected at the same time and detected by variant-specific forward primers.

(F) Quantification of the PAT assay in (E).

(G) Codon usage of leucine (Leu) codons in zebrafish. The bars show the occurrence of each Leu codon per 1,000 codons.

(H) Results of the time course PAT assay for reporter mRNAs containing the EGFP (CAI = 0.835) ORF with 21 CUG codons (upper, CUG × 21) and its variant in which all CUG codons were substituted with CUA codons (lower, CUA × 21).

(I) Quantification of the PAT assay in (E) at 6 hpf. See also Figure S5.

codons to the 3′ end of the mRNA, but not to the stop codon, as an insertion of UAG stop codon downstream of 5′-positioned uncommon codons did not restore deadenylation activity (Figures 5F–5H, 5′ low + stop). The positional effect was also observed with an independent, artificially designed ORF, albeit less evidently (Figures S5E and S5F).

To analyze the positional preference of uncommon codons in endogenous mRNAs, we calculated local CAI every 150 nt (50 codons) either from the 5′ or 3′ end of ORFs (Figure 5I). This analysis revealed two important features in addition to the global difference of CAI. First, the beginning of ORF generally shows the lowest local CAI regardless of the decay classes. This is consistent with the previously reported codon usage ramp conserved in three domains of life, which is considered to facilitate translation (Tuller et al., 2010). Second, the difference of local CAI between stable and M-decay mRNAs is more evident in the posterior regions of ORF, with the 3′-most regions showing the most significant difference. These observations are consistent with the distance model of codon-mediated decay, thus explaining how long 3′ UTRs confer resistance to codon-mediated deadenylation.

A Combinatory Impact of Codon Usage and 3′ UTR Length on the Maternal mRNA Stability

Having established codon usage bias and the 3′ UTR length as determinants of the deadenylation rate in zebrafish, we analyzed the influence of these two determinants on the stability of endogenous maternal mRNAs. We visualized the

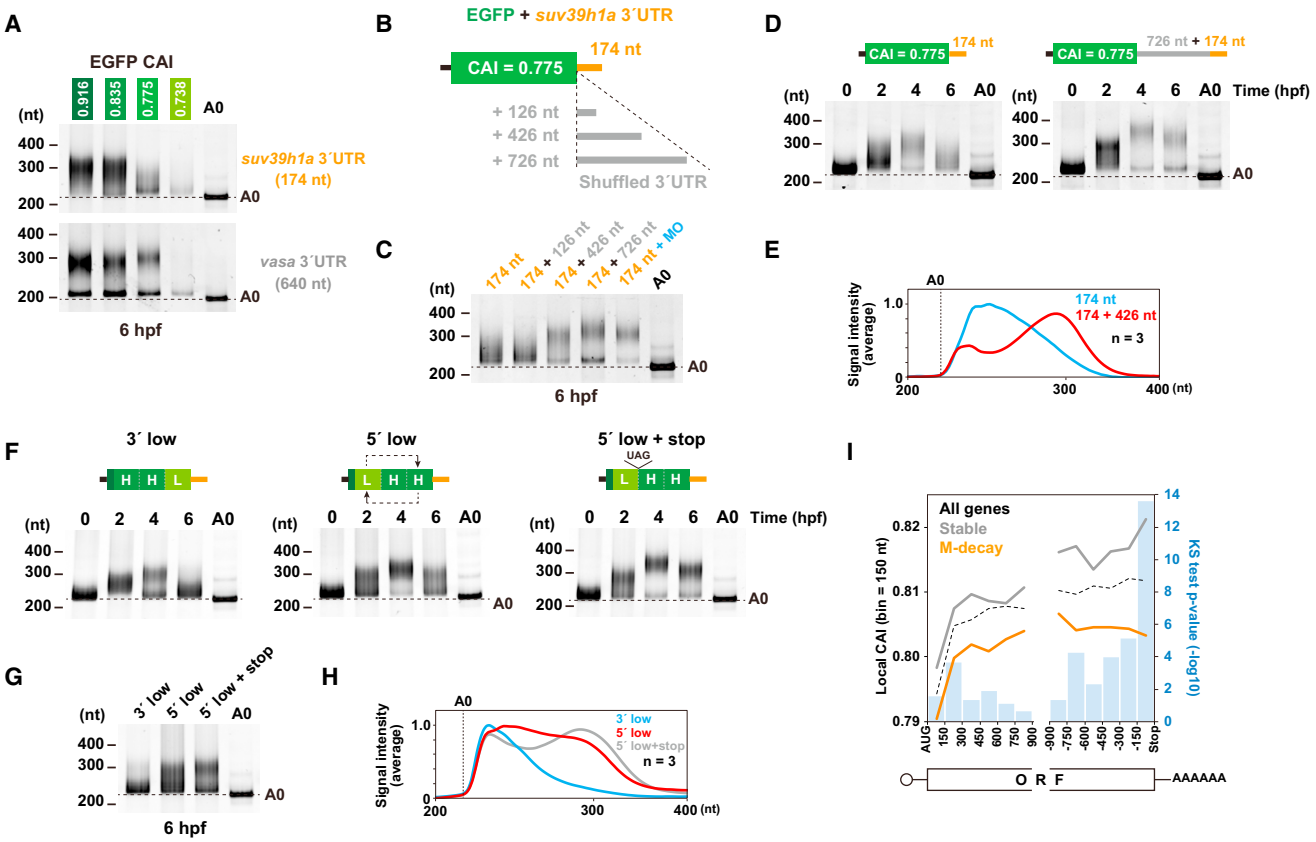

Figure 5. The Effect of 3′ UTR Length on Codon-Mediated Deadenylation

(A) Results of the PAT assay for reporter mRNAs containing EGFP ORF with differential synonymous codon usage (shown as green gradient; CAI is shown in white letters) and *suv39h1a* 3′ UTR (orange, upper panel) or *vasa* 3′ UTR (gray, lower panel) at 6 hpf. Lanes labeled as A0 show 3′ UTR fragments without a poly(A) tail.

(B) A schematic representation of the EGFP (CAI 0.775)-*suv39h1a* 3′ UTR reporter mRNA with 3′ UTR extension sequences of various lengths.

(C) Results of the PAT assay for EGFP (CAI 0.775)-*suv39h1a* 3′ UTR reporter mRNAs with various lengths of extension sequences at 6 hpf.

(D) Results of the time course PAT assay of EGFP (CAI 0.775)-*suv39h1a* 3′ UTR reporter mRNA (left) and EGFP (CAI 0.775)-726 nt-*suv39h1a* 3′ UTR reporter mRNA (right).

(E) Quantification of the PAT assays for EGFP (CAI 0.775) mRNAs with *suv39h1a* 3′ UTR alone (blue) or with 426 nt extension followed by *suv39h1a* 3′ UTR (red) at 6 hpf. The plots show the averaged relative signal intensity of three biological replicates (y axis) and the mobility (x axis).

(F) Results of the time course PAT assay of chimeric EGFP reporter mRNAs containing *suv39h1a* 3′ UTR. Left: the reporter mRNA whose 5′ two-thirds of the ORF are derived from EGFP (0.835) (dark green boxes labeled as "H") and whose 3′ one-third of the ORF is derived from EGFP (0.738) (a light green box labeled as "L"). Middle: a reporter mRNA containing swapped ORF fragments derived from the reporter mRNA shown on the left. Right: a reporter mRNA derived from the reporter mRNA in the middle, containing a stop codon insertion.

(G) PAT assay detecting the three constructs shown in (F) at 6 hpf.

(H) Quantification of the PAT assays in (G).

(I) Local CAI analysis of all genes (black dashed line), stable mRNAs (gray), and M-decay mRNAs (orange). The x axis shows positions of each bin relative to the start or stop codons, and the y axis on the left shows local CAI. The blue bars represent p values comparing stable mRNAs and M-decay mRNAs (y axis on the right, p values of two-sided Kolmogorov-Smirnov test, −log10 scale). See also Figure S5.

distribution of all or a subclass of genes based on the CAI and 3′ UTR length using the Kernel density estimation (Figures 6A–6C). The distribution of M-decay genes was biased toward a lower CAI and shorter 3′ UTR than the all genes background. Conversely, the distribution of stable genes was biased toward a higher CAI and longer 3′ UTR. We next divided the genes into four groups according to the median values (CAI 0.806 and 3′ UTR 570 nt) and analyzed the enrichment or depletion of genes in each group compared with the all gene background (Figures 6D–6F). Consistent with the Kernel density estimation, M-decay genes were the most enriched in the group with lower CAI and shorter 3′ UTR (41% of M-decay genes versus 25% of all genes, p = 5.7e−48, Fisher's exact test), whereas they were depleted from the group with higher CAI and longer 3′ UTR (14% of M-decay genes versus 26% of all genes, p = 9e−35). Stable genes were the most enriched in the group with higher CAI and longer 3′ UTR (36%, p = 9.7e−15), whereas these genes were depleted from the group with lower CAI and shorter 3′ UTR (15%, p = 2.6e−15). These transcriptome-wide analyses confirm the pervasive influence of codon usage and 3′ UTR on maternal mRNA stability during zebrafish MZT.

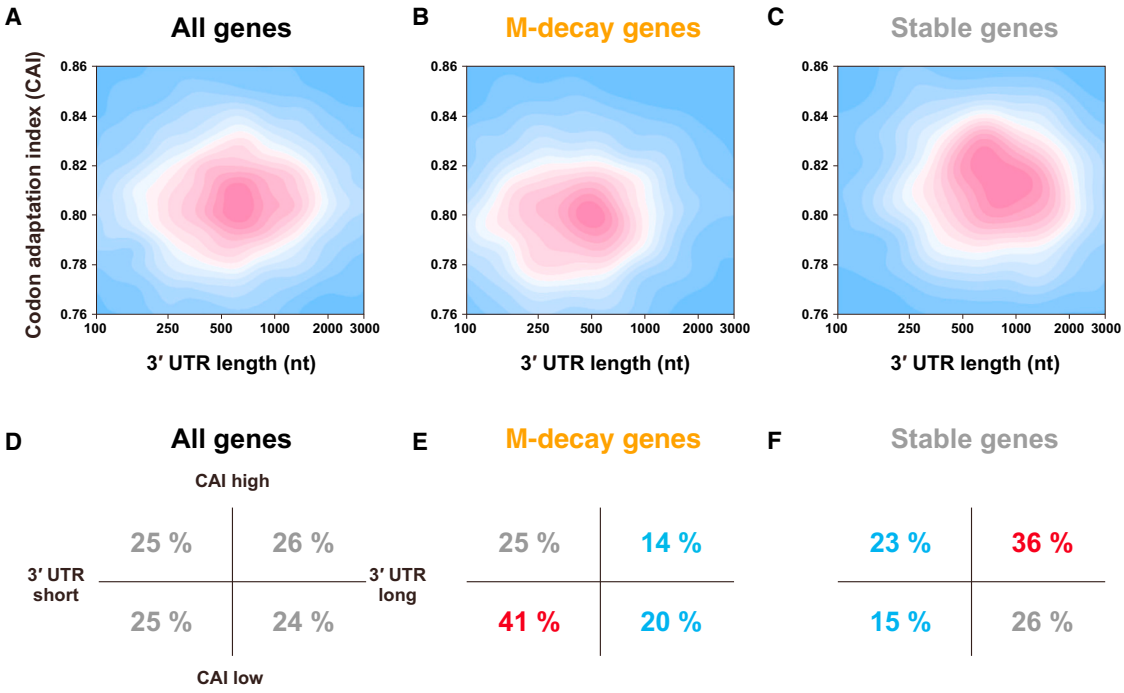

Figure 6. A Combinatory Impact of Codon Usage and 3′ UTR Length on the Maternal mRNA Stability

(A–C) Kernel density estimation maps of all genes (A), M-decay genes (B), and stable genes (C) based on the 3′ UTR length (x axis, log10 scale) and CAI (y axis). The local density of genes is color coded, with regions of high density shown in red and low density shown in blue.

(D–F) Distribution of all genes (D), M-decay genes (E) and stable genes (F) in four groups divided by median values (CAI 0.806 and 3′ UTR 570 nt). The percentages of genes in each group are shown; red indicates enrichment, and blue indicates depletion ($p < 0.01$, two-sided Fisher's exact test). See also Figures S5 and S6.

DISCUSSION

In the present study, we identified synonymous codon usage and 3′ UTR length as determinants of maternal mRNA stability in zebrafish. These determinants promote maternal mRNA clearance independently of ZGA, representing the maternal decay pathway whose molecular mechanism had been uncharacterized in vertebrates (Tadros and Lipshitz, 2009). Several observations highlight codon-mediated decay as a reasonable mechanism for promoting maternal mRNA clearance (Figure S6A). First, translation dependency of codon-mediated decay is suitable to promote maternal mRNA clearance after fertilization, because a majority of maternal mRNAs is stored in oocytes as a dormant form and their translation is activated upon fertilization (Weill et al., 2012; Krauchunas and Wolfner, 2013). Second, a preference of codon-mediated decay for short 3′ UTRs is consistent with the characteristic of maternal mRNAs, as maternal transcriptome is biased toward short 3′ UTRs in zebrafish (Ulitsky et al., 2012; Li et al., 2012). Third, codon-mediated decay complements the zygotic decay factor miR-430, which promotes maternal mRNA clearance in a sequence-dependent but translation-independent manner (Figures S4E and S4F) (Giraldez et al., 2006; Mishima et al., 2006). Although it is currently unknown if other Z-decay mRNAs are degraded cotranslationally, they tend to have longer 3′ UTRs and exhibit intermediate CAI (Figures 3C and S5G–S5I). These characteristics of Z-dacay mRNAs do not fit our codon-mediated M-decay model, implying that a distinct mechanism operates in the zygotic decay pathway. Further analysis will reveal whether codon-mediated decay is a conserved mode of maternal mRNA clearance in vertebrates.

The codon-mediated decay observed in zebrafish embryos is largely consistent with a recent report in yeast (Presnyak et al., 2015); both studies revealed that a subset of synonymous codons promotes mRNA degradation via the CCR4-NOT complex, while others confer mRNA stability. Hence, the two studies collectively indicate that codons play a conserved role for determining mRNA stability in eukaryotes. It should be noted, however, that the two studies utilized related but distinct metrics to define the two classes of codons. Presnyak et al. demonstrated that codons associated with mRNA instability are less optimal codons for translation based on the tRNA adaptive index (tAI), which infers tRNA availability from tRNA gene copy number and codon-anticodon pairing (dos Reis et al., 2004; Presnyak et al., 2015). By contrast, we focused on the codon usage bias in the zebrafish genome and demonstrated that uncommon synonymous codons promote mRNA deadenylation and degradation (Figure 4). Importantly, the codon optimality and the codon usage bias are not the same metrics; the former has been introduced as a direct proxy for the tRNA availability, whereas the latter is considered a consequence of multiple selective pressures including the tRNA availability (dos Reis et al., 2004; Pechmann and Frydman, 2013; Sharp and Li, 1987; Richter and Coller, 2015). As such, the identity of mRNA-stabilizing and destabilizing codons might be different between the two species. Further study is required to

determine what features of codons and corresponding tRNAs are recognized by the ribosome and how the difference leads to the opposite effects on mRNA stability.

Because codon usage not only affects the translation rate and mRNA stability but also affects cotranslational folding and protein localization, synonymous codon choice must be subject to significant evolutionary constraints (Pechmann and Frydman, 2013; Kim et al., 2015; Chaney and Clark, 2015; Yu et al., 2015). Hence, codon usage itself may be an intrinsic rather than a regulatory determinant of mRNA stability. Importantly, we demonstrated that 3′ UTR length is a modulator of codon-mediated decay (Figures 5 and S6B). This previously unrecognized function of 3′ UTR length is significant in two ways. First, long 3′ UTRs compensate for the constraint on synonymous codon usage, facilitating the stable expression of genes enriched with uncommon codons. Second, the modulatory role of the 3′ UTR length confers additional specificity to codon-mediated decay. Because codon-mediated deadenylation occurred efficiently when uncommon codons were placed in proximity to the 3′ end of the mRNA (Figures 5F–5I), we speculate that the topology of 3′ UTR (e.g., secondary structures and looping by the RNA-binding proteins) will also affect the efficiency of codon-mediated decay.

Several studies have indicated that long 3′ UTRs promote mRNA degradation. For example, long RNA sequences downstream of the stop codon promote NMD (Eberle et al., 2008; Behm-Ansmant et al., 2007; Singh et al., 2008; Hogg and Goff, 2010). Longer 3′ UTR isoforms, which are often generated by alternative polyadenylation (APA), embed more miRNA target sites and thereby negatively influence mRNA stability in cancer and proliferating cells (Mayr and Bartel, 2009; Sandberg et al., 2008). Our study revises these prevailing views by revealing that long 3′ UTRs act as an mRNA-stabilizing element in conjunction with the codon-mediated decay. Perhaps the effect of 3′ UTR length on mRNA stability is difficult to generalize when multiple regulatory mechanisms coexist. mRNA decay mechanisms may not be equally active in different cell types or status. A unique characteristic of zebrafish embryos before ZGA, in which miRNA expression is limited (Chen et al., 2005), might accentuate the mRNA-stabilizing effect of long 3′ UTRs in codon-mediated decay.

Finally, we predict that codon-mediated decay is dynamically controlled by multiple mechanisms. Recent studies have demonstrated that APA, which generates 3′ UTR isoforms with different lengths, is a widespread cotranscriptional regulatory mechanism in eukaryotes (Elkon et al., 2013). Thus, codon-mediated decay may be effective in one cell type but ineffective in another. Moreover, the tRNA repertoire varies depending on the tissues and cellular conditions (Dittmar et al., 2006; Gingold et al., 2014). Accordingly, decoding kinetics of each codon may vary in different tissues or conditions, thereby redirecting codon-mediated decay to a different set of target mRNAs. Future studies will reveal whether codon-mediated decay actively shapes gene expression patterns in conjunction with these mechanisms.

EXPERIMENTAL PROCEDURES

Microinjection

Fertilized eggs were obtained from the zebrafish AB strain by natural breeding. Microinjection was performed using an IM300 Microinjector (NARISHIGE). Approximately 1,000 pL of solution was injected per embryo within 15 min after fertilization. Embryos were developed in system water at 28.5°C.

qRT-PCR

Five to ten embryos were collected, and total RNA was prepared using TRI Reagent (Molecular Research Center). cDNA was synthesized from 450 ng of total RNA using the PrimeScript RT reagent kit with gDNA eraser (TAKARA). A random hexamer was used for cDNA synthesis to avoid detecting differences in the poly(A) tail length. qRT-PCR was performed using SYBR Premix Ex TaqII (Tli RNaseH Plus) and the Thermal Cycler Dice Real Time System (TAKARA). Specific amplification of the PCR products was confirmed after analyzing the dissociation curve, followed by gel electrophoresis and sequencing.

PAT Assay

PAT assay was performed using a poly(G) tailing method (Kusov et al., 2001) with some modifications. Briefly, 150 ng of total RNA were incubated with 75 U of yeast poly(A) polymerase (PAP) (Affymetrix) in the presence of 0.375 mM GTP and 0.125 mM ITP at 37°C for 60 min. cDNA was synthesized using the PrimeScript RT reagent kit with gDNA eraser (TAKARA) and a customized PAT primer (y300 PAT universal C10: 5′-GGTAATACGACTCAC TATAGCGAGACCCCCCCCCCTT-3′). cDNA synthesis was performed at 44°C for 15 min. PAT-PCR was performed using a gene-specific forward primer and y300 PAT universal C10 primes with GoTaq Green Master Mix (Promega). The control PCR was performed using a gene-specific forward primer and a reverse primer complementary to the annotated 3′ end, followed by the sequence of the y300 PAT primer. Experiments were repeated multiple times to confirm reproducibility.

RNA Sequencing

Total RNA was extracted from 40–50 embryos using TRI Reagent (Molecular Research Center), treated with DNase I (TAKARA), and purified using the RNeasy Mini Kit (QIAGEN). Libraries for RNA sequencing were prepared using TruSeq stranded total RNA with Ribo-Zero (Illumina). The libraries were multiplexed, and single-end sequencing was performed with Hiseq 2000 according to the manufacturer's instruction (Illumina). We sequenced triplicate RNA samples derived from three independent trials per condition.

ACCESSION NUMBERS

The accession number for the sequence data reported in this paper is GEO: GSE71609.

SUPPLEMENTAL INFORMATION

Supplemental Information includes Supplemental Experimental Procedures, six figures, and two tables and can be found with this article online at http://dx.doi.org/10.1016/j.molcel.2016.02.027.

AUTHOR CONTRIBUTIONS

Y.M. designed the project, performed the experiments, and analyzed the data. Y.M. and Y.T. interpreted the data and wrote the manuscript.

ACKNOWLEDGMENTS

We thank IMCB Research Center for Epigenetic Diseases for performing RNA sequencing. We are grateful to Cei-Abreu Goodger, Antonio Giraldez, and Ariel Bazzini for discussion; Kaori Kiyokawa for fish maintenance; and members of the Y.T. laboratory for assistance and comments on the project. This work was supported by a Grant-in-Aid for Young Scientists (B) (00557069) and Grants-in-Aid for Scientific Research on Innovative Areas "non-coding RNA" (24115711) to Y.M. and "non-coding RNA neo-taxonomy" (26113007) to Y.T. from the Ministry of Education, Culture, Sports, Science, and Technology. The Nakajima Foundation, the Mochida Memorial Foundation for Medical and Pharmaceutical Research, and the Daiichi-Sankyo Foundation of Life Science provided additional support to Y.M.

Received: November 5, 2015
Revised: January 25, 2016
Accepted: February 19, 2016
Published: March 17, 2016

REFERENCES

Bartel, D.P. (2009). MicroRNAs: target recognition and regulatory functions. Cell *136*, 215–233.

Bashirullah, A., Halsell, S.R., Cooperstock, R.L., Kloc, M., Karaiskakis, A., Fisher, W.W., Fu, W., Hamilton, J.K., Etkin, L.D., and Lipshitz, H.D. (1999). Joint action of two RNA degradation pathways controls the timing of maternal transcript elimination at the midblastula transition in Drosophila melanogaster. EMBO J. *18*, 2610–2620.

Basquin, J., Roudko, V.V., Rode, M., Basquin, C., Séraphin, B., and Conti, E. (2012). Architecture of the nuclease module of the yeast Ccr4-not complex: the Not1-Caf1-Ccr4 interaction. Mol. Cell *48*, 207–218.

Bazzini, A.A., Lee, M.T., and Giraldez, A.J. (2012). Ribosome profiling shows that miR-430 reduces translation before causing mRNA decay in zebrafish. Science *336*, 233–237.

Behm-Ansmant, I., Gatfield, D., Rehwinkel, J., Hilgers, V., and Izaurralde, E. (2007). A conserved role for cytoplasmic poly(A)-binding protein 1 (PABPC1) in nonsense-mediated mRNA decay. EMBO J. *26*, 1591–1601.

Bianchin, C., Mauxion, F., Sentis, S., Séraphin, B., and Corbo, L. (2005). Conservation of the deadenylase activity of proteins of the Caf1 family in human. RNA *11*, 487–494.

Braun, J.E., Huntzinger, E., Fauser, M., and Izaurralde, E. (2011). GW182 proteins directly recruit cytoplasmic deadenylase complexes to miRNA targets. Mol. Cell *44*, 120–133.

Bushati, N., Stark, A., Brennecke, J., and Cohen, S.M. (2008). Temporal reciprocity of miRNAs and their targets during the maternal-to-zygotic transition in Drosophila. Curr. Biol. *18*, 501–506.

Chaney, J.L., and Clark, P.L. (2015). Roles for synonymous codon usage in protein biogenesis. Annu. Rev. Biophys. *44*, 143–166.

Chekulaeva, M., Mathys, H., Zipprich, J.T., Attig, J., Colic, M., Parker, R., and Filipowicz, W. (2011). miRNA repression involves GW182-mediated recruitment of CCR4-NOT through conserved W-containing motifs. Nat. Struct. Mol. Biol. *18*, 1218–1226.

Chen, C.Y., and Shyu, A.B. (2011). Mechanisms of deadenylation-dependent decay. Wiley Interdiscip. Rev. RNA *2*, 167–183.

Chen, P.Y., Manninga, H., Slanchev, K., Chien, M., Russo, J.J., Ju, J., Sheridan, R., John, B., Marks, D.S., Gaidatzis, D., et al. (2005). The developmental miRNA profiles of zebrafish as determined by small RNA cloning. Genes Dev. *19*, 1288–1293.

Chen, C.Y., Zheng, D., Xia, Z., and Shyu, A.B. (2009). Ago-TNRC6 triggers microRNA-mediated decay by promoting two deadenylation steps. Nat. Struct. Mol. Biol. *16*, 1160–1166.

Collart, M.A., and Panasenko, O.O. (2012). The Ccr4—not complex. Gene *492*, 42–53.

De Renzis, S., Elemento, O., Tavazoie, S., and Wieschaus, E.F. (2007). Unmasking activation of the zygotic genome using chromosomal deletions in the Drosophila embryo. PLoS Biol. *5*, e117.

Decker, C.J., and Parker, R. (2012). P-bodies and stress granules: possible roles in the control of translation and mRNA degradation. Cold Spring Harb. Perspect. Biol. *4*, a012286.

Dittmar, K.A., Goodenbour, J.M., and Pan, T. (2006). Tissue-specific differences in human transfer RNA expression. PLoS Genet. *2*, e221.

dos Reis, M., Savva, R., and Wernisch, L. (2004). Solving the riddle of codon usage preferences: a test for translational selection. Nucleic Acids Res. *32*, 5036–5044.

Eberle, A.B., Stalder, L., Mathys, H., Orozco, R.Z., and Mühlemann, O. (2008). Posttranscriptional gene regulation by spatial rearrangement of the 3′ untranslated region. PLoS Biol. *6*, e92.

Elkon, R., Ugalde, A.P., and Agami, R. (2013). Alternative cleavage and polyadenylation: extent, regulation and function. Nat. Rev. Genet. *14*, 496–506.

Fabian, M.R., Cieplak, M.K., Frank, F., Morita, M., Green, J., Srikumar, T., Nagar, B., Yamamoto, T., Raught, B., Duchaine, T.F., and Sonenberg, N. (2011). miRNA-mediated deadenylation is orchestrated by GW182 through two conserved motifs that interact with CCR4-NOT. Nat. Struct. Mol. Biol. *18*, 1211–1217.

Gingold, H., Tehler, D., Christoffersen, N.R., Nielsen, M.M., Asmar, F., Kooistra, S.M., Christophersen, N.S., Christensen, L.L., Borre, M., Sørensen, K.D., et al. (2014). A dual program for translation regulation in cellular proliferation and differentiation. Cell *158*, 1281–1292.

Giraldez, A.J., Mishima, Y., Rihel, J., Grocock, R.J., Van Dongen, S., Inoue, K., Enright, A.J., and Schier, A.F. (2006). Zebrafish MiR-430 promotes deadenylation and clearance of maternal mRNAs. Science *312*, 75–79.

Hamatani, T., Carter, M.G., Sharov, A.A., and Ko, M.S. (2004). Dynamics of global gene expression changes during mouse preimplantation development. Dev. Cell *6*, 117–131.

Hogg, J.R., and Goff, S.P. (2010). Upf1 senses 3'UTR length to potentiate mRNA decay. Cell *143*, 379–389.

Ivshina, M., Lasko, P., and Richter, J.D. (2014). Cytoplasmic polyadenylation element binding proteins in development, health, and disease. Annu. Rev. Cell Dev. Biol. *30*, 393–415.

Jonas, S., and Izaurralde, E. (2013). The role of disordered protein regions in the assembly of decapping complexes and RNP granules. Genes Dev. *27*, 2628–2641.

Jonas, S., and Izaurralde, E. (2015). Towards a molecular understanding of microRNA-mediated gene silencing. Nat. Rev. Genet. *16*, 421–433.

Kane, D.A., and Kimmel, C.B. (1993). The zebrafish midblastula transition. Development *119*, 447–456.

Kim, S.J., Yoon, J.S., Shishido, H., Yang, Z., Rooney, L.A., Barral, J.M., and Skach, W.R. (2015). Protein folding. Translational tuning optimizes nascent protein folding in cells. Science *348*, 444–448.

Krauchunas, A.R., and Wolfner, M.F. (2013). Molecular changes during egg activation. Curr. Top. Dev. Biol. *102*, 267–292.

Kusov, Y.Y., Shatirishvili, G., Dzagurov, G., and Gauss-Müller, V. (2001). A new G-tailing method for the determination of the poly(A) tail length applied to hepatitis A virus RNA. Nucleic Acids Res. *29*, E57.

Li, Y., Sun, Y., Fu, Y., Li, M., Huang, G., Zhang, C., Liang, J., Huang, S., Shen, G., Yuan, S., et al. (2012). Dynamic landscape of tandem 3′ UTRs during zebrafish development. Genome Res. *22*, 1899–1906.

Lykke-Andersen, J., and Bennett, E.J. (2014). Protecting the proteome: eukaryotic cotranslational quality control pathways. J. Cell Biol. *204*, 467–476.

Makino, S., Mishima, Y., Inoue, K., and Inada, T. (2015). Roles of mRNA fate modulators Dhh1 and Pat1 in TNRC6-dependent gene silencing recapitulated in yeast. J. Biol. Chem. *290*, 8331–8347.

Mathavan, S., Lee, S.G., Mak, A., Miller, L.D., Murthy, K.R., Govindarajan, K.R., Tong, Y., Wu, Y.L., Lam, S.H., Yang, H., et al. (2005). Transcriptome analysis of zebrafish embryogenesis using microarrays. PLoS Genet. *1*, 260–276.

Mayr, C., and Bartel, D.P. (2009). Widespread shortening of 3'UTRs by alternative cleavage and polyadenylation activates oncogenes in cancer cells. Cell *138*, 673–684.

Mishima, Y., Giraldez, A.J., Takeda, Y., Fujiwara, T., Sakamoto, H., Schier, A.F., and Inoue, K. (2006). Differential regulation of germline mRNAs in soma and germ cells by zebrafish miR-430. Curr. Biol. *16*, 2135–2142.

Paillard, L., Omilli, F., Legagneux, V., Bassez, T., Maniey, D., and Osborne, H.B. (1998). EDEN and EDEN-BP, a cis element and an associated factor that mediate sequence-specific mRNA deadenylation in Xenopus embryos. EMBO J. *17*, 278–287.

Pechmann, S., and Frydman, J. (2013). Evolutionary conservation of codon optimality reveals hidden signatures of cotranslational folding. Nat. Struct. Mol. Biol. *20*, 237–243.

Petit, A.P., Wohlbold, L., Bawankar, P., Huntzinger, E., Schmidt, S., Izaurralde, E., and Weichenrieder, O. (2012). The structural basis for the interaction between the CAF1 nuclease and the NOT1 scaffold of the human CCR4-NOT deadenylase complex. Nucleic Acids Res. *40*, 11058–11072.

Presnyak, V., Alhusaini, N., Chen, Y.H., Martin, S., Morris, N., Kline, N., Olson, S., Weinberg, D., Baker, K.E., Graveley, B.R., and Coller, J. (2015). Codon optimality is a major determinant of mRNA stability. Cell *160*, 1111–1124.

Richter, J.D., and Coller, J. (2015). Pausing on polyribosomes: make way for elongation in translational control. Cell *163*, 292–300.

Sandberg, R., Neilson, J.R., Sarma, A., Sharp, P.A., and Burge, C.B. (2008). Proliferating cells express mRNAs with shortened 3′ untranslated regions and fewer microRNA target sites. Science *320*, 1643–1647.

Sandler, H., Kreth, J., Timmers, H.T., and Stoecklin, G. (2011). Not1 mediates recruitment of the deadenylase Caf1 to mRNAs targeted for degradation by tristetraprolin. Nucleic Acids Res. *39*, 4373–4386.

Semotok, J.L., Cooperstock, R.L., Pinder, B.D., Vari, H.K., Lipshitz, H.D., and Smibert, C.A. (2005). Smaug recruits the CCR4/POP2/NOT deadenylase complex to trigger maternal transcript localization in the early Drosophila embryo. Curr. Biol. *15*, 284–294.

Sharp, P.M., and Li, W.H. (1987). The codon Adaptation Index—a measure of directional synonymous codon usage bias, and its potential applications. Nucleic Acids Res. *15*, 1281–1295.

Shi, Y., and Manley, J.L. (2015). The end of the message: multiple protein-RNA interactions define the mRNA polyadenylation site. Genes Dev. *29*, 889–897.

Singh, G., Rebbapragada, I., and Lykke-Andersen, J. (2008). A competition between stimulators and antagonists of Upf complex recruitment governs human nonsense-mediated mRNA decay. PLoS Biol. *6*, e111.

Stoeckius, M., Grün, D., Kirchner, M., Ayoub, S., Torti, F., Piano, F., Herzog, M., Selbach, M., and Rajewsky, N. (2014). Global characterization of the oocyte-to-embryo transition in Caenorhabditis elegans uncovers a novel mRNA clearance mechanism. EMBO J. *33*, 1751–1766.

Subtelny, A.O., Eichhorn, S.W., Chen, G.R., Sive, H., and Bartel, D.P. (2014). Poly(A)-tail profiling reveals an embryonic switch in translational control. Nature *508*, 66–71.

Suzuki, A., Igarashi, K., Aisaki, K., Kanno, J., and Saga, Y. (2010). NANOS2 interacts with the CCR4-NOT deadenylation complex and leads to suppression of specific RNAs. Proc. Natl. Acad. Sci. USA *107*, 3594–3599.

Tadros, W., and Lipshitz, H.D. (2009). The maternal-to-zygotic transition: a play in two acts. Development *136*, 3033–3042.

Tadros, W., Goldman, A.L., Babak, T., Menzies, F., Vardy, L., Orr-Weaver, T., Hughes, T.R., Westwood, J.T., Smibert, C.A., and Lipshitz, H.D. (2007). SMAUG is a major regulator of maternal mRNA destabilization in Drosophila and its translation is activated by the PAN GU kinase. Dev. Cell *12*, 143–155.

Tuller, T., Carmi, A., Vestsigian, K., Navon, S., Dorfan, Y., Zaborske, J., Pan, T., Dahan, O., Furman, I., and Pilpel, Y. (2010). An evolutionarily conserved mechanism for controlling the efficiency of protein translation. Cell *141*, 344–354.

Ulitsky, I., Shkumatava, A., Jan, C.H., Subtelny, A.O., Koppstein, D., Bell, G.W., Sive, H., and Bartel, D.P. (2012). Extensive alternative polyadenylation during zebrafish development. Genome Res. *22*, 2054–2066.

Weill, L., Belloc, E., Bava, F.A., and Méndez, R. (2012). Translational control by changes in poly(A) tail length: recycling mRNAs. Nat. Struct. Mol. Biol. *19*, 577–585.

Yu, C.H., Dang, Y., Zhou, Z., Wu, C., Zhao, F., Sachs, M.S., and Liu, Y. (2015). Codon usage influences the local rate of translation elongation to regulate co-translational protein folding. Mol. Cell *59*, 744–754.

Zheng, D., Ezzeddine, N., Chen, C.Y., Zhu, W., He, X., and Shyu, A.B. (2008). Deadenylation is prerequisite for P-body formation and mRNA decay in mammalian cells. J. Cell Biol. *182*, 89–101.